# Epithelial control of colonisation by *Streptococcus pneumoniae* at the human mucosal surface

Caroline M Weight*[1], Cristina Venturini[1], Sherin Pojar[2], Simon P. Jochems[2], Jesús Reiné[2], Elissavet Nikolaou[2], Carla Solórzano[2], Mahdad Noursadeghi[1], Jeremy S Brown[3], Daniela M. Ferreira[2], Robert S Heyderman[1]

[1]Division of Infection and Immunity, University College London, London, United Kingdom, [2]Department of Clinical Sciences, Liverpool School of Tropical Medicine, Liverpool, United Kingdom, [3]Department of Respiratory Medicine, University College London, London, United Kingdom

**Corresponding Author*: Dr Caroline M. Weight, Division of Infection and Immunity, The Rayne Building, 5 University Street, University College London, WC1E 6JF, UK.

Email: c.weight@ucl.ac.uk; Tel: +44 20 3108 2351

## ABSTRACT

Control of *Streptococcus pneumoniae* colonisation at human mucosal surfaces is critical to reducing the burden of pneumonia and invasive pneumococcal disease, interrupting transmission, and achieving herd protection. Using an Experimental Human Pneumococcal Carriage Model (EHPC), we show that *S. pneumoniae* colonisation is associated with epithelial surface adherence, microcolony formation and invasion, without overt disease. Interactions between different strains and the epithelium *in vitro* shaped the host transcriptomic response. Using epithelial modules from a human epithelial cell model that recapitulates our *in vivo* findings, comprising innate signalling/ regulatory pathways, inflammatory mediators, cellular metabolism and stress response genes, we find that inflammation in the EHPC model is most prominent around the time of bacterial clearance. These results show that rather than being confined to the epithelial surface and the overlying mucus layer, the pneumococcus undergoes micro-invasion that enhances the inflammatory/ innate immune response associated with clearance which may also trigger transmission.

48 Colonisation of upper respiratory tract (URT) mucosa by a range of pathogenic bacteria is a
49 necessary precursor to both disease and onward transmission. Although *Streptococcus pneumoniae*
50 is a common coloniser of the human nasopharynx, it is estimated to be responsible for >500,000
51 deaths due to pneumonia, meningitis and sepsis in children under five years of age worldwide[1].
52
53 In Europe and North America, there has been a dramatic effect of pneumococcal conjugate vaccine
54 (PCV) on vaccine serotype (VT) invasive disease, carriage and transmission[2]. However, the
55 emergence of non-VT pneumococcal disease worldwide and the more modest impact of PCV on
56 colonisation in high transmission settings, threaten this success[3]. Control of pneumococcal URT
57 colonisation in humans is not fully understood[4], and so defining the mechanistic basis for host control
58 of pneumococcal colonisation at the mucosal surface is therefore crucial for the further optimisation
59 of therapeutic interventions which target carriage and transmission.
60
61 Naturally acquired immunity to pneumococcal antigens is primarily mediated by mucosal T cells,
62 anti-protein antibodies, controlled by Treg[5,6]. The URT epithelium is central to this process[7], binding
63 and transporting antibodies, sensing bacteria via a range of surface and intracellular pathogen-
64 associated molecular patterns (PAMPs) receptors, and rapidly transducing signals to recruit innate
65 and inflammatory immune mechanisms[8,9].
66
67 Murine models suggest that adherence of *S. pneumoniae* to the mucosal epithelium may be followed
68 by paracellular transmigration and tight junction modulation[10,11]. In contrast, studies of immortalised
69 epithelial cell monolayers implicate endocytosis of *S. pneumoniae*, mediated though pneumococcal
70 protein C–polymeric immunoglobulin receptor interactions[12,13]. The relative importance of epithelial
71 endocytosis and paracellular migration in colonisation and invasion remains uncertain[13], but could
72 influence epithelial sensing of this otherwise extracellular pathogen[11]. This may include TLR2
73 signalling via lipoteichoic acid[14,15], Nod1 signalling via peptidoglycan[16] and TLR4 signalling via
74 pneumolysin, a pore-forming toxin that induces inflammation and mediates both clearance and
75 transmission in an infant mouse model[17-19].

We have explored the hypothesis that pneumococcal-epithelial engagement dictates the inflammatory/ innate immune response and therefore the outcome of colonisation. Much of what we understand of the control of pneumococcal colonisation is derived from epidemiological studies and murine carriage models. The experimental human pneumococcal carriage (EHPC) model provides a well-controlled, reproducible tool to characterise the cellular and molecular mechanisms that underlie pneumococcal colonisation in humans[20]. We have used human epithelial cell lines and different strains of *S. pneumoniae* to further probe these mechanisms and derive epithelial transcriptome module to interrogate the host response in the EHPC model. We show that pneumococcal colonisation in humans is characterised by microcolony formation, junctional protein association and migration across the epithelial barrier without disease, which we have termed micro-invasion. This pattern of bacterial-host cell association shapes epithelial sensing of *S. pneumoniae,* which is partially pneumolysin dependent. Together, our data suggest that pneumococcal engagement with the epithelium in the early phases of colonisation may occur without eliciting a marked host response. As colonisation becomes more established, epithelial sensing of *S. pneumoniae* enhances innate immunity/ inflammation which we propose promotes clearance and may trigger transmission.

## RESULTS

### Pneumococcal colonisation of the human nasopharynx is associated with epithelial adhesion, microcolony formation and micro-invasion

We have used an EHPC model[21] to capture the epithelial events central to pneumococcal colonisation, obtaining human mucosal samples by curette biopsy. We defined a carrier as an individual colonised by 6B *S. pneumoniae* as detected by culture of nasal wash at any day following

102 inoculation. Clearance was defined as when *S. pneumoniae* colonisation became negative by culture
103 of nasal wash.
104
105 Colonisation was detected in 9/13 healthy volunteers by culture, 12/13 by microscopy and 9/11 by
106 LytA PCR (Table 1). Carriage was detected by culture/ PCR at day 2, whereas maximum detection
107 by microscopy was evident at day 6. This is not explained by colonisation density and therefore the
108 sensitivity of culture/ PCR. This could be explained by greater association with the epithelium
109 (detected by all techniques) rather than the overlying mucus (detected by culture/PCR but not
110 microscopy) over time. Clearance generally occurred between day 9 and day 27 (Table 1 and Figure
111 1b).
112
113 Curette biopsy samples visualised by confocal microscopy using Wheat Germ Agglutinin (WGA) as
114 a marker for surface carbohydrates and Junctional Adhesion Molecule A (JAM-A) as a marker of
115 tight junctions, yielded intact sheets of epithelial cells associated with polymorphonuclear leukocytes,
116 characterised morphologically (Figure 1a and Supplementary Figure 1a). Amongst carriers,
117 pneumococci were found on the epithelial surface (Table 1; Figure 1c, Figure 1d) which over time
118 became associated with microcolony formation (Figure 1e). There was evidence of pneumococcal
119 invasion of the epithelial monolayer ("micro-invasion", Figure 1e-f). Pneumococci were also
120 observed in phagocytic cells (Supplementary Figure 1a). Colonisation was frequently characterised
121 by co-association between *S. pneumoniae* and JAM-A (Figure 1f). This intimate association between
122 inoculated pneumococci and the mucosa in the EHPC model is suggestive of an active process that
123 reflects natural asymptomatic pneumococcal carriage in humans.
124
125 **Epithelial surface marker expression *in vivo* is not altered in response to colonisation with *S.***
126 ***pneumoniae***
127 To determine whether pneumococcal colonisation leads to epithelial activation, we analysed nasal
128 curette biopsy cells for surface expression of EpCAM (epithelial cell identification), IL-22Ra1,
129 HLADR, CD40, CD54 and CD107a (Supplementary Figure 2a-d). We did not detect a significant
130 change in the relative expression of IL-22Ra1 (protects the epithelial barrier, promotes anti-microbial

131 product secretion during infection, modulating pneumococcal carriage and clearance[22]), HLADR
132 (mediates T cell-antigen recognition and is a marker of epithelial activation[23]), CD40 (co-stimulatory
133 protein which binds CD154[24] (Supplementary Figure 2e-g)) or CD54 (a leukocyte adhesion molecule
134 which is also upregulated by CD40[24,25], initiating neutrophil migration and recruitment[26]) (Figure 2a).
135 However, although numbers of epithelial cells expressing CD107a did not change over time (Figure
136 2b), we observed an increase in CD107a$^{high}$ expression at day 2 post inoculation in carriage positive
137 volunteers vs. carriage negative volunteers (Figure 2b). CD107a in the epithelium forms the
138 membrane glycoprotein of late endosomes and phagolysosomes[13] and has previously been
139 implicated in pneumococcal endocytosis[13]. These data highlight the ability of the pneumococcus to
140 colonise the nasopharynx without marked inflammation and potentially implicate CD107a in the
141 process.

142

143 ***S. pneumoniae* infection of nasopharyngeal epithelial cells *in vitro* is associated with**
144 **pneumococcal adhesion, microcolony formation and micro-invasion**

145 To further understand epithelial responses to *S. pneumoniae* observed in the EHPC model, we
146 undertook infection experiments with Detroit 562 epithelial cells. We compared the 6B response with
147 two other representative clinical isolates, TIGR4 (the original sequenced strain[27]) and 23F, and a
148 TIGR4 pneumolysin deletion mutant strain (dPly).

149

150 TIGR4 association with Detroit 562 cells was over 100-fold higher for adhesion and over 70-fold
151 higher for invasion after three hours infection, compared to 6B or 23F strains (Figure 3a-b).
152 Pneumococcal adhesion to the epithelial surface was associated with microcolony formation and
153 internalisation of this conventionally extracellular pathogen[11] (Figure 3d-e, Supplementary Figure
154 3a). Intracellular pneumococci were contained within intracellular vesicles suggestive of endocytosis,
155 which was most marked with the TIGR4 strain (Figure 3b)[13]. Intracellular pneumococci were coated
156 with JAM-A (Figure 3f, Supplementary Figure 3a) and associated with the adherens junction protein
157 β catenin but not Claudin 4 (Supplementary Figure 3a). Pneumococci were located laterally,
158 transiting between cell junctions (Figure 3g), at the level of the nuclei and below the basal membrane

159 (Figure 3h). Transmigration across the epithelium (endocytosis or paracellular movement), as
160 measured by the culture of pneumococci from the basal chamber of transwell inserts, was most
161 marked with 23F (Figure 3c, five-fold higher compared to TIGR4, after three hours infection). A
162 similar pattern of epithelial interaction was also seen at one hour suggesting these observations are
163 not simply explained by differential growth.

164

165 Epithelial infection with the dPly-TIGR4 mutant showed a significant increase in adherence (Figure
166 3a, ten-fold higher after three hours infection), internalisation (Figure 3b, three-fold higher after three
167 hours infection), but no significant differences in transmigration (Figure 3c) compared to the wild-
168 type strain, implicating pneumolysin in the modulation of bacterial interactions with the epithelium.

169

170 Similar patterns of adherence and invasion were observed in infection experiments with human
171 Calu3 and A549 epithelial cells demonstrating that these findings are cell-line independent
172 (Supplementary Figure 4). Furthermore, primary epithelial cells differentiated on an air-liquid
173 interface for 30 days and co-cultured with either 6B or 23F *S. pneumoniae* also revealed
174 pneumococcal microcolony formation, micro-invasion and epithelial junctional protein association
175 (Supplementary Figure 1b).

176

177 Together these data show the strain dependency of pneumococcal-epithelial interactions *in vitro*
178 which mirror the pathways for epithelial micro-invasion seen *in vivo*.

179

180 **Endocytosis-related micro-invasion and transmigration**

181 To confirm that the pneumococcal endocytosis leads to transmigration across the epithelium,
182 endocytosis was inhibited with dynasore and nystatin[13]. After one hour of infection, cellular uptake
183 of 23F was inhibited by 82% (Figure 4a) and transmigration across the cell monolayer by 85% (Figure
184 4b). This inhibition of endocytosis and transmigration was also seen with TIGR4 (data not shown).

185 In agreement with previous studies using A549 and Calu3 cells[28], we found that viable pneumococci
186 in Detroit 562 cells decreased over time (Supplementary Figure 5a). Using gentamicin treatment to
187 eliminate the original extracellular inoculum, we observed *S. pneumoniae* in the apical and basal
188 media (Supplementary Figure 5b), suggesting egress from the epithelium.

189

190 **Loss of epithelial cell barrier function is not a pre-requisite for micro-invasion by *S.***
191 ***pneumoniae***

192 *S. pneumoniae* has been shown to affect the integrity of epithelial barriers and tight junction function
193 in murine models[10,29]. Having demonstrated pneumococcal micro-invasion without obvious epithelial
194 morphological disruption, we explored possible effects on epithelial barrier function by measuring
195 trans-epithelial electrical resistance (TEER) and permeability to 4kDa FITC-dextran in Detroit 562
196 cells. TEER was not adversely affected by pneumococcal co-culture (Figure 4c) and permeability
197 was maintained with all the pneumococcal strains at three hours post-infection (Figure 4d). Although
198 co-localisation of pneumococci was seen with host proteins, we did not detect marked epithelial
199 membrane carbohydrate or protein re-distribution (WGA, Claudin 4 JAM-A, β catenin,
200 Supplementary Figure 3a). Similar observations were made with A549 cells and Calu3 cells
201 (Supplementary Figure 4). These data suggest that pneumococcal micro-invasion was not
202 dependent on loss of epithelial cell barrier function during early interactions.

203

204 ***S. pneumoniae* upregulates epithelial surface CD54 and CD107a *in vitro***

205 In a similar manner to primary cells collected from nasal curettes, we assessed Detroit 562 cell
206 surface marker expression in response to *S. pneumoniae* (Supplementary Figure 6a-c). There were
207 no significant changes in IL-22Ra1, HLADR or CD40 expression in response to 6B, 23F, TIGR4 and
208 dPly-TIGR4 strains (Supplementary Figure 6d-e). However, $CD54^{high}$ expression was significantly
209 greater in response to the TIGR4 and dPly-TIGR4 strains, compared to non-infected cells (Figure
210 5a). Epithelial CD107a was upregulated in response to the 6B, 23F and TIGR4 strains (Figure 5b),
211 but this was not seen with dPly-TIGR4. These data implicate pneumolysin in the induction of CD107a

212 but not CD54 epithelial surface expression and support the possibility that CD107a is involved in
213 pneumococcal-epithelial micro-invasion events seen *in vivo*.

214

215 **_Streptococcus pneumoniae_ induces epithelial secretion of IL-6, IL-8 and CD54**

216 To assess the inflammatory consequences of pneumococcal-epithelial infections *in vitro*, we
217 measured a cytokine panel in Detroit 562 cell supernatants following *S. pneumoniae* incubation
218 (Figure 5c). We detected a significant increase in IL-6 and IL-8, which were strain dependent and
219 partially pneumolysin dependent. In line with surface marker observations, only TIGR4 significantly
220 upregulated the secretion of soluble CD54, which was dependent on pneumolysin (Figure 5c). These
221 data highlight the less inflammatory nature of the 6B strain compared to the more invasive strain,
222 TIGR4, and the importance of pneumolysin in the epithelial response. Pneumococcal wild-type strain
223 differences were not explained by differences in pneumolysin activity, as determined by hemolysis
224 (Supplementary Figure 7).

225

226 **Innate transcriptomic responses to epithelial infection by _S. pneumoniae in vitro_**

227 To explore the hypothesis that the pattern of epithelial adhesion and micro-invasion results in
228 differential epithelial responses, we performed RNAseq of Detroit 562 cells infected with our panel
229 of *S. pneumoniae* strains. In comparison to non-infected epithelial cell cultures (Figure 6a), infection
230 with TIGR4 upregulated expression of 1127 genes (550 unique genes), 23F upregulated 650 genes
231 (69 unique genes), and 6B upregulated 153 genes (10 unique genes). The pneumolysin deficient
232 isogenic mutant of TIGR4 upregulated 220 genes (14 unique genes). Compared to non-infected
233 cells, 1193 genes were upregulated by *S. pneumoniae* infection overall and 93 were core to all
234 strains tested.

235

236 To elucidate the pathways that drive the transcriptional responses to each strain, we also undertook
237 transcription factor binding site enrichment analysis (Figure 6b, Online Supplementary File). The
238 responses to 6B and pneumolysin deficient strains were principally enriched in binding sites for the

239 NFkB/Rel family of transcription factors, indicating that an NFkB activation pathway was the
240 dominant driver for responses to these strains. In contrast, cellular responses to TIGR4 and 23F
241 strains revealed enriched binding sites for more diverse transcription factors, suggesting diverse
242 molecular pathways by which these strains may influence cellular function. This analysis revealed
243 particular enrichment of binding sites for beta-beta-alpha zinc finger superfamily of transcription
244 factors, including SP1 and KLF4, suggesting that these strains upregulate mitogen activated protein
245 kinase pathways upstream of these transcription factors[30].

246

247 The sets of genes upregulated by each strain individually were subjected to core and interactome
248 and pathway-enrichment analysis for functional annotation of the cellular response at systems level
249 (Figure 6c, Online Supplementary File). From 20 clusters of pathways, significant enrichment of
250 innate immune system responses was evident in all strains and included specific enrichment in Toll
251 receptor cascades, peptide ligand-binding receptors, NFkB and MAP kinase activation, Interferon
252 signalling and cytokine and chemokine signalling, (Figure 6c, 6d). In general, the greater number of
253 transcripts upregulated by TIGR4 and 23F strains compared to 6B translated to a larger number of
254 biological pathways with differential innate immune responses to each strain (Figure 6c). Fewer
255 transcriptional responses at the level of functional pathways in response to dPly-TIGR4 is consistent
256 with a role for pneumolysin in innate immune recognition of *S. pneumoniae*[31]. Fewer transcriptional
257 responses to 6B is consistent with our observations that this strain exhibits the lowest level of cellular
258 association and transmigration.

259

260 **Epithelial transcriptomic responses to 6B are detectable *in vivo***

261 Next, we sought to test whether these epithelial transcriptomic responses to *S. pneumoniae* were
262 also evident in the 6B EHPC model. We compared nasal transcriptomes sampled at two or nine days
263 after inoculation to pre-inoculation samples. These revealed significant enrichment of 158 transcripts
264 among individuals who became colonised (Supplementary Figure 9). These genes included Claudin
265 5 and Claudin 17, Defensin β 103A/B, Cadherin 16, Desmocollin 1 and Gap junction protein α1,

266 which suggests cytoskeletal re-organisation two days post-inoculation in carriage positive
267 individuals. At day 9 post-inoculation, innate molecules such as CCR3, matrix metalloproteinase 12
268 and MHC II molecules were enriched, suggesting innate activation. However, these gene sets were
269 not significantly enriched for any immune response pathway annotation perhaps because of the
270 statistical stringency necessary for genome-wide multiple testing and were not epithelial-specific.

271

272 Gene expression modules can successfully detect specific transcriptional programs in bulk tissue[32].
273 Therefore, as an alternative approach, we sought to target specific epithelial responses *in vivo* using
274 the *in vitro* interactome. A direct comparison of transcripts for 6B revealed FOSL-1, an AP-1
275 transcription factor subunit, to be enriched with carriage. To expand the sensitivity of the approach,
276 we evaluated the expression of two transcriptional modules in the nasal samples (Figure 7). A 'core'
277 module comprised of 16 interacting genes (Figure 7b) that were upregulated in the Detroit epithelium
278 by all the pneumococcal strains from Figure 7a, and a second 'integrated' module that comprised of
279 200 interacting genes (Figure 7c), which were upregulated in the Detroit epithelium by at least one
280 of the pneumococcal strains from Figure 7a. Among carriage negative individuals, we found no
281 increase in expression in either gene expression modules (Figure 7b-c). In contrast among the
282 individuals who became colonised, the expression of both modules, but significantly increased within
283 the integrated module (Figure 7b,7c), suggests that the prominence of responses at day nine may
284 reflect time-dependent proliferation of the 6B bacterial inoculum and the subsequent epithelial
285 interactions. These responses coincide around the time of bacterial clearance.

286

287

288 **DISCUSSION**

289 It is widely accepted that colonisation of the URT mucosa by many potentially pathogenic bacterial
290 species, involves transient association with the overlying mucus layer but that adherence to the
291 epithelial surface avoids mucus entrapment and muco-ciliary clearance[11,33]. While evading immunity,
292 bacterial replication then occurs prior to onward transmission to a new host. Even for *S. pneumoniae,*

293 the mechanisms underlying this transition from acquisition to established colonisation, and then
294 transmission and/or disease, are not well understood. By combining an EHPC model and *in vitro*
295 human cell culture systems, we show that pneumococcal colonisation leads to epithelial adherence,
296 microcolony formation and migration across the epithelial barrier without disease, which we have
297 termed micro-invasion. The finding of co-association with junctional proteins provides a possible
298 mechanism for micro-invasion. Clearance of the pneumococcus from the mucosa *in vivo* occurs in
299 the context of micro-invasion. Indeed, epithelial micro-invasion and not bacterial load *per s*e, appears
300 to dictate unique transcription factor binding site signatures, downstream cytokine, chemokine and
301 metabolic pathway enrichment (Figure 8).

302

303 The concept of mucosal micro-invasion moves us away from current models of colonisation where
304 the pneumococcus is held up at the epithelial surface and that invasion leads to disease. Our data
305 are supported by murine colonisation experiments[34,35] and the detection of pneumococcal DNA in
306 blood of otherwise healthy, colonised children[36]. In line with other cell culture and murine
307 models[10,13,34,37], we have demonstrated that pneumococcal micro-invasion occurs by endocytosis
308 through the formation of cytoplasmic vacuoles, and by paracellular transcytosis across the
309 epithelium. Micro-invasion of the epithelium may overcome the inaccessibility of PAMP receptors
310 located either at the epithelial basolateral surface or intracellularly[38,39]. We have found that at early
311 time points, micro-invasion *in vitro* is also characterised by pneumococcal co-association with JAM-
312 A and β catenin without evidence of barrier dysfunction. In murine models at later time points, TLR-
313 dependent Claudin 7 and Claudin 10 down-regulation enhanced pneumococcal translocation across
314 the epithelium has been observed[10]. While this may occur as inflammation becomes more prominent,
315 our data suggest that micro-invasion can happen without barrier disruption and that the epithelium
316 plays an active role in the regulation of these complex host-pathogen interactions[9].

317

318 The differential impact of micro-invasion on the epithelial transcriptomic response was striking with
319 considerable enrichment of multiple diverse transcription factors and signalling pathways related to

320 innate immunity with the most invasive pneumococcal strains. The interactome module highlights
321 that although enrichment of gene activation in response to all pneumococcal strains is apparent (the
322 core module), a more diverse range of epithelial gene activation occurs between strains, reflecting
323 specific host-pathogen interactions. Nasal colonisation in murine models is proinflammatory[40,41], but
324 our *in vitro* and EHPC experiments with serotype 6B suggests this is not always the case, whereby
325 pneumococcal-host cell adherence, growth, endocytosis and paracellular migration can be
326 established without a marked host response. In the EHPC, clearance occurred around the time the
327 epithelial transcriptomic response was most prominent. Weiser and colleagues argue that the
328 colonising pneumococcus induces the host response that mediates clearance, but also promotes
329 nutrient acquisition and onward transmission[11,17,42], which is supported by murine models[43] and
330 epidemiological studies of viral-coinfection[44]. The enrichment of binding sites for SP1 and KLF4
331 transcription factors seen in our *in vitro* data suggests a counter-regulatory process aimed at
332 minimising inflammation. KLF4 plays a role in barrier function, suppression of NFκB-dependent IL-8
333 secretion, regulation of IL-10 expression via TLR9-MyD88 and Yes-1, in response to *S. pneumoniae,*
334 which is partially dependent on autolysin LytA[30,45,46]. Thus, by exploiting micro-invasion, the
335 pneumococcus may carefully calibrate the host innate immune/ inflammatory response to promote
336 survival through transmission.
337

338 A range of pneumococcal PAMPs including pneumolysin, may trigger this epithelial sensing
339 process[17,47]. We found pneumolysin to be a prominent influencer of epithelial surface molecule
340 upregulation, cytokine production and transcriptomic inflammatory response *in vitro*. Mediated by
341 autolysin, the pneumococcus undergoes autolysis during stationery growth phase, resulting in
342 additional PAMPs' release including bacterial DNA. In mice, pneumococcal DNA triggers
343 inflammation through a DAI/STING/TBK1/IRF3 cascade[40,48], a response that may contribute to
344 pneumococcal clearance. In our *in vitro* transcriptomic analyses, we detected enriched activation of
345 IRF3/IFR7 in dPly-TIGR4. We suggest that in the context of micro-invasion, pneumococcal DNA
346 may act as a trigger of epithelial sensing, inducing inflammation[48].
347

348 Our findings are limited by the pneumococcal strains available for testing in the EHPC model to
349 enable direct comparisons with *in vitro* data. Nonetheless, the use of different strains *in vitro* has
350 enabled us and others[49,50] to determine the impact of different patterns of epithelial adherence and
351 invasion on the host inflammatory/ innate immune response. Our findings are also supported by *ex*
352 *vivo* primary cell cultures in an air-liquid interface derived from the EHPC, and by the EHPC itself.

353

354 In conclusion, our data implicates the novel finding of micro-invasion during pneumococcal
355 colonisation of otherwise healthy humans. Micro-invasion may influence the outcome of colonisation
356 by altering the balance between innate immunity/ inflammation-driven transmission and clearance.
357 This balance may be further modulated by the frequency of carriage events, pneumococcal strain
358 co-colonisation, viral co-infections and other environmental pressures[1,43]. The pathways critical for
359 onward pneumococcal transmission remain to be determined in humans. Our approach combining
360 *in vitro* with *in vivo* human systems offers a potentially tractable way to interrogate this question.

361

362

363 **ACKNOWLEDGEMENTS**

364 This study was funded by the Wellcome Trust (Grant 106846/Z/15/Z). DF is supported by the Medical
365 Research Council (grant MR/M011569/1), Bill and Melinda Gates Foundation (grant OPP1117728)
366 and the National Institute for Health Research (NIHR) Local Comprehensive Research Network.
367 LytA PCR was performed by Prof. D Bogaert, University of Edinburgh, UK. RNAseq library
368 preparation undertaken at either UCL through the Pathogens Genomic Unit or at the Wellcome
369 Sanger Institute, Hinxton with thanks to Carl Anderson. Confocal imaging facilities at LSTM were
370 funded by a Wellcome Trust Multi-User Equipment Grant (104936/Z/14/Z). Flow cytometric
371 acquisition was funded by a Wellcome Trust Multi-User Equipment Grant (104936/Z/14/Z).

372

373 **AUTHOR CONTRIBUTIONS**: CMW, SPJ, DMF and RSH conceived and designed the study. CMW,
374 SP, SPJ, JR, EN, CS acquired the data. CMW, CV, SPJ, MN, JSB, DMF, RSH analysed and

interpreted the data. CMW wrote the first draft of the manuscript. CMW, CV, SP, SPJ, JR, EN, CS, MN, JSB, DMF, RSH commented on and approved the manuscript.

**COMPETING INTERESTS:** The authors declare no competing financial interests.

## REFERENCES


1 O'Brien, K. L. *et al.* Burden of disease caused by Streptococcus pneumoniae in children younger than 5 years: global estimates. *Lancet* **374**, 893-902, doi:10.1016/S0140-6736(09)61204-6 (2009).

2 Whitney, C. G. *et al.* Decline in invasive pneumococcal disease after the introduction of protein-polysaccharide conjugate vaccine. *N Engl J Med* **348**, 1737-1746, doi:10.1056/NEJMoa022823 (2003).

3 Hanage, W. P. *et al.* Carried pneumococci in Massachusetts children: the contribution of clonal expansion and serotype switching. *Pediatr Infect Dis J* **30**, 302-308, doi:10.1097/INF.0b013e318201a154 (2011).

4 Jochems, S. P., Weiser, J. N., Malley, R. & Ferreira, D. M. The immunological mechanisms that control pneumococcal carriage. *PLoS Pathog* **13**, e1006665, doi:10.1371/journal.ppat.1006665 (2017).

5 Pido-Lopez, J., Kwok, W. W., Mitchell, T. J., Heyderman, R. S. & Williams, N. A. Acquisition of pneumococci specific effector and regulatory Cd4+ T cells localising within human upper respiratory-tract mucosal lymphoid tissue. *PLoS Pathog* **7**, e1002396, doi:10.1371/journal.ppat.1002396 (2011).

6 Zhang, Q. *et al.* Characterisation of regulatory T cells in nasal associated lymphoid tissue in children: relationships with pneumococcal colonization. *PLoS Pathog* **7**, e1002175, doi:10.1371/journal.ppat.1002175 (2011).

7 Ratner, A. J., Lysenko, E. S., Paul, M. N. & Weiser, J. N. Synergistic proinflammatory responses induced by polymicrobial colonization of epithelial surfaces. *Proc Natl Acad Sci U S A* **102**, 3429-3434, doi:10.1073/pnas.0500599102 (2005).

8 Eisele, N. A. & Anderson, D. M. Host Defense and the Airway Epithelium: Frontline Responses That Protect against Bacterial Invasion and Pneumonia. *J Pathog* **2011**, 249802, doi:10.4061/2011/249802 (2011).

9 Whitsett, J. A. & Alenghat, T. Respiratory epithelial cells orchestrate pulmonary innate immunity. *Nat Immunol* **16**, 27-35, doi:10.1038/ni.3045 (2015).

10 Clarke, T. B., Francella, N., Huegel, A. & Weiser, J. N. Invasive bacterial pathogens exploit TLR-mediated downregulation of tight junction components to facilitate translocation across the epithelium. *Cell Host Microbe* **9**, 404-414, doi:10.1016/j.chom.2011.04.012 (2011).

11 Weiser, J. N., Ferreira, D. M. & Paton, J. C. Streptococcus pneumoniae: transmission, colonization and invasion. *Nat Rev Microbiol* **16**, 355-367, doi:10.1038/s41579-018-0001-8 (2018).

12 Agarwal, V., Asmat, T. M., Dierdorf, N. I., Hauck, C. R. & Hammerschmidt, S. Polymeric immunoglobulin receptor-mediated invasion of Streptococcus pneumoniae into host cells requires a coordinate signaling of SRC family of protein-tyrosine kinases, ERK, and c-Jun N-terminal kinase. *J Biol Chem* **285**, 35615-35623, doi:10.1074/jbc.M110.172999 (2010).

13 Asmat, T. M., Agarwal, V., Saleh, M. & Hammerschmidt, S. Endocytosis of Streptococcus pneumoniae via the polymeric immunoglobulin receptor of epithelial cells relies on clathrin and caveolin dependent mechanisms. *Int J Med Microbiol* **304**, 1233-1246, doi:10.1016/j.ijmm.2014.10.001 (2014).

420 14 Beisswenger, C., Coyne, C. B., Shchepetov, M. & Weiser, J. N. Role of p38 MAP kinase and
421 transforming growth factor-beta signaling in transepithelial migration of invasive bacterial
422 pathogens. *J Biol Chem* **282**, 28700-28708, doi:10.1074/jbc.M703576200 (2007).
423 15 Tomlinson, G. *et al.* TLR-mediated inflammatory responses to Streptococcus pneumoniae are highly
424 dependent on surface expression of bacterial lipoproteins. *J Immunol* **193**, 3736-3745,
425 doi:10.4049/jimmunol.1401413 (2014).
426 16 Ratner, A. J., Aguilar, J. L., Shchepetov, M., Lysenko, E. S. & Weiser, J. N. Nod1 mediates cytoplasmic
427 sensing of combinations of extracellular bacteria. *Cell Microbiol* **9**, 1343-1351, doi:10.1111/j.1462-
428 5822.2006.00878.x (2007).
429 17 Zafar, M. A., Wang, Y., Hamaguchi, S. & Weiser, J. N. Host-to-Host Transmission of Streptococcus
430 pneumoniae Is Driven by Its Inflammatory Toxin, Pneumolysin. *Cell Host Microbe* **21**, 73-83,
431 doi:10.1016/j.chom.2016.12.005 (2017).
432 18 Malley, R. *et al.* Recognition of pneumolysin by Toll-like receptor 4 confers resistance to
433 pneumococcal infection. *Proc Natl Acad Sci U S A* **100**, 1966-1971 (2003).
434 19 Ratner, A. J. *et al.* Epithelial cells are sensitive detectors of bacterial pore-forming toxins. *J Biol Chem*
435 **281**, 12994-12998, doi:10.1074/jbc.M511431200 (2006).
436 20 Ferreira, D. M. *et al.* Controlled human infection and rechallenge with Streptococcus pneumoniae
437 reveals the protective efficacy of carriage in healthy adults. *Am J Respir Crit Care Med* **187**, 855-864,
438 doi:10.1164/rccm.201212-2277OC (2013).
439 21 Wright, A. K. *et al.* Human nasal challenge with Streptococcus pneumoniae is immunising in the
440 absence of carriage. *PLoS Pathog* **8**, e1002622, doi:10.1371/journal.ppat.1002622 (2012).
441 22 Trevejo-Nunez, G., Elsegeiny, W., Conboy, P., Chen, K. & Kolls, J. K. Critical Role of IL-22/IL22-RA1
442 Signaling in Pneumococcal Pneumonia. *J Immunol* **197**, 1877-1883, doi:10.4049/jimmunol.1600528
443 (2016).
444 23 Fais, S. *et al.* HLA-DR antigens on colonic epithelial cells in inflammatory bowel disease: I. Relation to
445 the state of activation of lamina propria lymphocytes and to the epithelial expression of other surface
446 markers. *Clin Exp Immunol* **68**, 605-612 (1987).
447 24 Propst, S. M., Denson, R., Rothstein, E., Estell, K. & Schwiebert, L. M. Proinflammatory and Th2-
448 derived cytokines modulate CD40-mediated expression of inflammatory mediators in airway
449 epithelia: implications for the role of epithelial CD40 in airway inflammation. *J Immunol* **165**, 2214-
450 2221 (2000).
451 25 Cagnoni, F. *et al.* CD40 on adult human airway epithelial cells: expression and proinflammatory
452 effects. *J Immunol* **172**, 3205-3214 (2004).
453 26 Frick, A. G. *et al.* Haemophilus influenzae stimulates ICAM-1 expression on respiratory epithelial cells.
454 *J Immunol* **164**, 4185-4196 (2000).
455 27 Tettelin, H. *et al.* Complete genome sequence of a virulent isolate of Streptococcus pneumoniae.
456 *Science* **293**, 498-506, doi:10.1126/science.1061217 (2001).
457 28 Asmat, T. M., Agarwal, V., Rath, S., Hildebrandt, J. P. & Hammerschmidt, S. Streptococcus
458 pneumoniae infection of host epithelial cells via polymeric immunoglobulin receptor transiently
459 induces calcium release from intracellular stores. *J Biol Chem* **286**, 17861-17869,
460 doi:10.1074/jbc.M110.212225 (2011).
461 29 Peter, A. *et al.* Localization and pneumococcal alteration of junction proteins in the human alveolar-
462 capillary compartment. *Histochem Cell Biol* **147**, 707-719, doi:10.1007/s00418-017-1551-y (2017).
463 30 Herta, T. *et al.* DNA-release by Streptococcus pneumoniae autolysin LytA induced Krueppel-like
464 factor 4 expression in macrophages. *Sci Rep* **8**, 5723, doi:10.1038/s41598-018-24152-1 (2018).
465 31 Malley, R. *et al.* Recognition of pneumolysin by Toll-like receptor 4 confers resistance to
466 pneumococcal infection. *Proc Natl Acad Sci U S A* **100**, 1966-1971, doi:10.1073/pnas.0435928100
467 (2003).
468 32 Pollara, G. *et al.* Validation of Immune Cell Modules in Multicellular Transcriptomic Data. *PLoS One*
469 **12**, e0169271, doi:10.1371/journal.pone.0169271 (2017).
470 33 Siegel, S. J. & Weiser, J. N. Mechanisms of Bacterial Colonization of the Respiratory Tract. *Annu Rev*
471 *Microbiol* **69**, 425-444, doi:10.1146/annurev-micro-091014-104209 (2015).

472 34 Mahdi, L. K., Ogunniyi, A. D., LeMessurier, K. S. & Paton, J. C. Pneumococcal virulence gene expression
473 and host cytokine profiles during pathogenesis of invasive disease. *Infect Immun* **76**, 646-657,
474 doi:10.1128/IAI.01161-07 (2008).
475 35 Briles, D. E., Novak, L., Hotomi, M., van Ginkel, F. W. & King, J. Nasal colonization with Streptococcus
476 pneumoniae includes subpopulations of surface and invasive pneumococci. *Infect Immun* **73**, 6945-
477 6951, doi:10.1128/IAI.73.10.6945-6951.2005 (2005).
478 36 Morpeth, S. C. *et al.* Detection of Pneumococcal DNA in Blood by Polymerase Chain Reaction for
479 Diagnosing Pneumococcal Pneumonia in Young Children From Low- and Middle-Income Countries.
480 *Clin Infect Dis* **64**, S347-S356, doi:10.1093/cid/cix145 (2017).
481 37 Talbot, U. M., Paton, A. W. & Paton, J. C. Uptake of Streptococcus pneumoniae by respiratory
482 epithelial cells. *Infect Immun* **64**, 3772-3777 (1996).
483 38 Gewirtz, A. T., Navas, T. A., Lyons, S., Godowski, P. J. & Madara, J. L. Cutting edge: bacterial flagellin
484 activates basolaterally expressed TLR5 to induce epithelial proinflammatory gene expression. *J*
485 *Immunol* **167**, 1882-1885 (2001).
486 39 Hornef, M. W., Wick, M. J., Rhen, M. & Normark, S. Bacterial strategies for overcoming host innate
487 and adaptive immune responses. *Nat Immunol* **3**, 1033-1040, doi:10.1038/ni1102-1033 (2002).
488 40 Koppe, U. *et al.* Streptococcus pneumoniae stimulates a STING- and IFN regulatory factor 3-
489 dependent type I IFN production in macrophages, which regulates RANTES production in
490 macrophages, cocultured alveolar epithelial cells, and mouse lungs. *J Immunol* **188**, 811-817,
491 doi:10.4049/jimmunol.1004143 (2012).
492 41 Wilson, R. *et al.* Protection against Streptococcus pneumoniae lung infection after nasopharyngeal
493 colonization requires both humoral and cellular immune responses. *Mucosal Immunol* **8**, 627-639,
494 doi:10.1038/mi.2014.95 (2015).
495 42 Zafar, M. A., Kono, M., Wang, Y., Zangari, T. & Weiser, J. N. Infant Mouse Model for the Study of
496 Shedding and Transmission during Streptococcus pneumoniae Monoinfection. *Infect Immun* **84**,
497 2714-2722, doi:10.1128/IAI.00416-16 (2016).
498 43 Plotkowski, M. C., Puchelle, E., Beck, G., Jacquot, J. & Hannoun, C. Adherence of type I Streptococcus
499 pneumoniae to tracheal epithelium of mice infected with influenza A/PR8 virus. *Am Rev Respir Dis*
500 **134**, 1040-1044, doi:10.1164/arrd.1986.134.5.1040 (1986).
501 44 Pittet, L. A., Hall-Stoodley, L., Rutkowski, M. R. & Harmsen, A. G. Influenza virus infection decreases
502 tracheal mucociliary velocity and clearance of Streptococcus pneumoniae. *Am J Respir Cell Mol Biol*
503 **42**, 450-460, doi:10.1165/rcmb.2007-0417OC (2010).
504 45 Zahlten, J. *et al.* Role of Pneumococcal Autolysin for KLF4 Expression and Chemokine Secretion in
505 Lung Epithelium. *Am J Respir Cell Mol Biol* **53**, 544-554, doi:10.1165/rcmb.2014-0024OC (2015).
506 46 Zahlten, J. *et al.* TLR9- and Src-dependent expression of Krueppel-like factor 4 controls interleukin-
507 10 expression in pneumonia. *Eur Respir J* **41**, 384-391, doi:10.1183/09031936.00196311 (2013).
508 47 Hotomi, M., Yuasa, J., Briles, D. E. & Yamanaka, N. Pneumolysin plays a key role at the initial step of
509 establishing pneumococcal nasal colonization. *Folia Microbiol (Praha)* **61**, 375-383,
510 doi:10.1007/s12223-016-0445-z (2016).
511 48 Parker, D. *et al.* Streptococcus pneumoniae DNA initiates type I interferon signaling in the respiratory
512 tract. *MBio* **2**, e00016-00011, doi:10.1128/mBio.00016-11 (2011).
513 49 Bootsma, H. J., Egmont-Petersen, M. & Hermans, P. W. Analysis of the in vitro transcriptional
514 response of human pharyngeal epithelial cells to adherent Streptococcus pneumoniae: evidence for
515 a distinct response to encapsulated strains. *Infect Immun* **75**, 5489-5499, doi:10.1128/IAI.01823-06
516 (2007).
517 50 Novick, S. *et al.* Adhesion and invasion of Streptococcus pneumoniae to primary and secondary
518 respiratory epithelial cells. *Mol Med Rep* **15**, 65-74, doi:10.3892/mmr.2016.5996 (2017).
519 51 Browall, S. *et al.* Intraclonal variations among Streptococcus pneumoniae isolates influence the
520 likelihood of invasive disease in children. *J Infect Dis* **209**, 377-388, doi:10.1093/infdis/jit481 (2014).
521 52 McCool, T. L., Cate, T. R., Moy, G. & Weiser, J. N. The immune response to pneumococcal proteins
522 during experimental human carriage. *J Exp Med* **195**, 359-365 (2002).

523 53 Hyams, C., Camberlein, E., Cohen, J. M., Bax, K. & Brown, J. S. The Streptococcus pneumoniae capsule
524 inhibits complement activity and neutrophil phagocytosis by multiple mechanisms. *Infect Immun* **78**,
525 704-715, doi:10.1128/IAI.00881-09 (2010).
526 54 Collins, A. M. *et al.* First human challenge testing of a pneumococcal vaccine. Double-blind
527 randomized controlled trial. *Am J Respir Crit Care Med* **192**, 853-858, doi:10.1164/rccm.201503-
528 0542OC (2015).
529 55 Jochems, S. P. *et al.* Novel Analysis of Immune Cells from Nasal Microbiopsy Demonstrates Reliable,
530 Reproducible Data for Immune Populations, and Superior Cytokine Detection Compared to Nasal
531 Wash. *PLoS One* **12**, e0169805, doi:10.1371/journal.pone.0169805 (2017).
532 56 Bray, N. L., Pimentel, H., Melsted, P. & Pachter, L. Near-optimal probabilistic RNA-seq quantification.
533 *Nat Biotechnol* **34**, 525-527, doi:10.1038/nbt.3519 (2016).
534 57 Soneson, C., Love, M. I. & Robinson, M. D. Differential analyses for RNA-seq: transcript-level
535 estimates improve gene-level inferences. *F1000Res* **4**, 1521, doi:10.12688/f1000research.7563.2
536 (2015).
537 58 Varet, H., Brillet-Gueguen, L., Coppee, J. Y. & Dillies, M. A. SARTools: A DESeq2- and EdgeR-Based R
538 Pipeline for Comprehensive Differential Analysis of RNA-Seq Data. *PLoS One* **11**, e0157022,
539 doi:10.1371/journal.pone.0157022 (2016).
540 59 Chakraborty, S., Datta, S. & Datta, S. Surrogate variable analysis using partial least squares (SVA-PLS)
541 in gene expression studies. *Bioinformatics* **28**, 799-806, doi:10.1093/bioinformatics/bts022 (2012).
542 60 Fang, H., Knezevic, B., Burnham, K. L. & Knight, J. C. XGR software for enhanced interpretation of
543 genomic summary data, illustrated by application to immunological traits. *Genome Med* **8**, 129,
544 doi:10.1186/s13073-016-0384-y (2016).

545
546
547

548 **METHODS**

549

550 **Bacteria**

551 *S. pneumoniae* clinical strains used were 6B (BHN 418[51]), 23F (P1121[52]) and TIGR4 (P1672[53]),
552 together with a pneumolysin deficient TIGR4 mutant strain (kind gift from Prof T Mitchell, University
553 of Birmingham). Stocks of bacterial aliquots grown to $O.D._{600nm}$ 0.3 were stored at -80$^{o}$C, defrosted,
554 resuspended in cell culture media and used once. Colony forming units (CFU) were counted on
555 horse blood agar plates (EO Labs).

556

557 **Experimental Human Pneumococcal Carriage Model (EHPC)**

558 Following written informed consent, healthy non-smoking adults between the ages of 18 – 59 were
559 inoculated with 80,000 CFU/nostril live 6B *S. pneumoniae* (BHN418), grown to mid-log phase in
560 vegetone broth as previously described[54]. Individuals naturally colonised with *S. pneumoniae* or in
561 regular contact with at-risk individuals were excluded. Nasal washes and mucosal cells (curette
562 biopsy) from the inferior turbinate were obtained by PBS syringe and curettage using a plastic Rhino-

563 probe™ (Arlington Scientific), in this order of collection respectively, before pneumococcal
564 inoculation. Sampling was then repeated on days 2, 6, 9, and 14 - 27 post pneumococcal
565 inoculation[55]. Volunteers received the TIV vaccine intramuscularly at day 3 post pneumococcal
566 inoculation. Bacteria collected from nasal washes were quantified by CFU counts. At each time-
567 point, two curettage samples were obtained and processed for confocal immunofluorescence, flow
568 cytometry, primary cell culture and /or transcriptomic analysis by RNA sequencing (RNAseq). There
569 were no adverse events. The carriage status of each volunteer was blinded until sample analysis
570 was completed.
571 Ethical approval was given by NHS Research and Ethics Committee (REC)/Liverpool School of
572 Tropical Medicine (LSTM) REC, reference numbers: 15/NW/0146 and 14/NW/1460 and Human
573 Tissue Authority licensing number 12548.
574
575 **Human Respiratory Tract Epithelial Cell Lines**
576 Human pharyngeal carcinoma Detroit 562 epithelial cells (ATCC_CCL-138) and human bronchial
577 carcinoma Calu3 epithelial cells (ATCC_HTB-55) were grown in 10% FCS in alpha MEM media
578 (Gibco). Human alveolar epithelial carcinoma A549 epithelial cells (ATCC_CCL-185) were grown in
579 10% FCS with 1% L-glutamine in Hams/F-12 media (Gibco).
580
581 **Pneumococcal-epithelial cell co-culture**
582 *Association and Invasion assays* - confluent Detroit 562 (typically day 8 post plating), Calu3 (typically
583 day 10 post plating) and A549 (typically day 4 post plating) monolayers cultured on 12 well plates
584 (Corning), were exposed to *S. pneumoniae* for three hours in 1% FCS alpha MEM (~MOI
585 approximately 1 cell : 10 pneumococci). The medium was removed, and cells washed three times in
586 $HBSS^{+/+}$. Cells were incubated in 1% saponin for 10 minutes at 37°C and lysed by repetitive pipetting.
587 Dilutions of bacteria were plated on blood agar and colonies counted after 16 hours. To quantify
588 internalised bacteria, 100µg/ml gentamicin was added for 1 hour to the cells, which were then
589 washed another three times, before incubating with 1% Saponin and plating on blood agar plates.
590 CFUs were counted after 16 hours incubation at 37°C, 5% $CO_2$. There were no differences in

591 pneumococcal pre- or post-inoculum, or growth density between the strains, in the cell supernatant
592 three hours post-infection.
593
594 *Transmigration assay* - Detroit 562 cells were cultured on 3µm pore, PET Transwell Inserts
595 (ThermoFisher) typically for 10 days to achieve confluent, polarised monolayers. Calu3 cells were
596 plated onto Transwell inserts typically for 12 days and A549 cells typically for 6 days. Cell culture
597 media was changed 1 hour prior to addition of bacteria to 1% FCS (250µl apical chamber, 1ml basal
598 chamber). Resistance was recorded before and after *S. pneumoniae* were added using an EVOM2
599 (World Precision Instruments). 1mg/ml FITC-dextran (Sigma Aldrich) was added to the apical
600 chamber of selected inserts to assess permeability. Approximately 12 million bacteria were added
601 to the cells (~MOI 1 cell : 25 bacteria). During the time course, 50µl was removed, diluted and plated,
602 from the basal chamber to measure bacterial load by counting CFU/well. Permeability was recorded
603 using a FLUOstar Omega (BMG Labtech) at 488nm.
604
605 *Endocytosis inhibition assays* - Detroit 562 cells cultured on 12 well plates were treated with 100µM
606 dynasore (Cambridge Biosciences) and 7.5µg/ml nystatin (Sigma Aldrich) to block endocytosis for
607 30 minutes prior to, and for the duration of pneumococcal infection incubation period. DMSO was
608 used as a control. Cells were washed and treated with gentamicin and lysed with saponin as
609 described above.
610
611 **Confocal Microscopy**
612 For the *in vivo* analysis, mucosal cells derived by curettage from the EHPC model were placed
613 directly into 4% PFA for 1 hour. Cells were cytospun onto microscope slides and allowed to air dry.
614 For the *in vitro* analysis, epithelial cell lines on transwell membranes were fixed in either 4% PFA
615 (Pierce, Methanol Free) or 1:1 mix of methanol:acetone for 20 minutes. Cells were permeabilised
616 with 0.2% Triton X-100 for 10 minutes and blocked for 1 hour in blocking buffer (3% goat serum and
617 3% BSA in PBS) before incubation with anti-6B pneumococcal antisera, JAM-A, Claudin-4 or β-
618 catenin primary antibodies (see Supplementary Information) for one hour and then secondary and/or
619 conjugated antibodies for 45 minutes. DAPI solution was added for 5 minutes. After washing, the

620 stained samples were mounted using Aqua PolyMount (VWR International) with a coverslip onto a
621 microslide. The entire cytospin for each sample was manually viewed by microscopy for detection of
622 pneumococci. Multiple fields of view (>3) were imaged for each transwell insert, for each condition.
623 Images were captured using either an inverted LSM 700, LSM 880, or TissueFAXS Zeiss Confocal
624 Microscope. Z stacks were recorded at 1µm intervals at either 40x oil or 63x oil objectives. For the
625 *in vivo* samples, the operator (CMW) was blinded to the colonisation status of the volunteer at the
626 time of sampling.
627
628
629 **Flow cytometry**
630 For the *in vivo* analysis, cells from two curette samples were incubated in cold PBS++ (PBS
631 supplemented with 5mM EDTA and 0.5% FCS) were dislodged by pipetting and centrifuged at 440g
632 for 5 mins at 4$^{o}$C. Supernatant was removed, and cells resuspended in 25µl of PBS++ with
633 Live/Dead$^{TM}$ Fixable Violet Dead Cell Stain (ThermoFisher). After 15 minutes incubation on ice, an
634 antibody cocktail to stain for epithelial surface marker expression (see Supplementary Information)
635 was added and incubated for another 15 minutes. Samples were vortexed, resuspended in 3.5mls
636 of PBS++ and filtered over a pre-wetted 70µm filter. Samples were transferred to a 5ml FACS tube,
637 centrifuged and resuspended in 200µl Cell Fix (BD Biosciences) and acquired on LSRII Flow
638 Cytometer (BD Biosciences). Compensation was run and applied for each experimental replicate
639 and voltages consistent throughout. Isotype controls (Biolegend) and FL-1 controls were also run for
640 each antibody. Analyses of data was performed using FlowJo LLC version 10 software. Data was
641 performed on the gated epithelial cell population and only samples containing 500 or more cells are
642 reported.
643
644 For the *in vitro* analysis, confluent monolayers of Detroit 562 cells on 6 well plates were incubated
645 with *S. pneumoniae* for 6 hours in 1% FCS phenol free alpha MEM (base media, Life Technologies).
646 Cells were washed three times in PBS and gently lifted from the plate using a cell scraper in 300µl
647 of base media supplemented with 1mM EDTA. Samples were transferred to 5ml FACS tubes and
648 placed on ice for the duration of the protocol. Each cell sample was incubated with an antibody

649 cocktail for epithelial surface marker expression (see Supplemental Information) for 30 minutes
650 before rinsing in 1ml base media and centrifuging at 300g for 5 minutes at 4°C. Cells were fixed in
651 600µl of 4% PFA and acquired on a LSR II Flow Cytometer (BD Biosciences). Compensation was
652 run and applied for each experimental replicate and voltages consistent throughout. Isotype controls
653 (BD Biosciences), FL-1 and single stains were also run for each experiment. Samples were acquired
654 until 300,000 events had been collected. Analyses were performed using FlowJo LLC version 10
655 software.
656
657
658 **ELISAs**
659 Supernatant from Detroit 562 cells that had been incubated with *S. pneumoniae* for 6 hours, was
660 collected for cytokine analysis. IL-1β, IL-6, IL-8, IFNγ, TNFα, ICAM-1 DuoSet® ELISA kits were
661 purchased from R&D Systems and protocol followed according to manufacturers' instructions.
662
663 **RNA samples and sequencing (RNASeq)**

664 Mucosal curettage samples and epithelial cell cultures (incubated with or without *S. pneumoniae* for
665 3 hours) were collected in RNALater (ThermoFisher) and stored at -80°C. RNA Extraction was
666 performed using the RNEasy micro kit (Qiagen) and genomic DNA was removed with on column
667 DNA digestion or with the Turbo DNA-free Kit (Qiagen). Extracted RNA quality was assessed and
668 quantified using a BioAnalyser (Agilent 2100). Library preparation and RNA-sequencing (Illumina
669 Hiseq4000, 20M reads, 100 paired-end reads) were performed at the Beijing Genome Institute
670 (China) or the Sanger Institute (UK) for mucosal curettage samples. For the Detroit 562 samples,
671 library preparation was performed using the Kappa Hyperprep kit (Roche Diagnostics) and
672 sequencing was performed by the Pathogens Genomic Unit (UCL) on the Illumina Nextseq using
673 the Nextseq 500/550 High Output 75 cycle kit (Illumina) according to manufacturers' instructions,
674 giving 15-20 million 41bp paired end reads per sample.

675

676 All data processing and analysis was conducted in R, language and environment for statistical
677 computing (https://www.R-project.org). Paired end reads were mapped to the Ensembl human
678 transcriptome reference sequence (homo sapiens GRCh38). Mapping and generation of read counts
679 per transcript were performed using Kallisto[56], based on pseudoalignment. R/Bioconductor package
680 Tximport was used to import the mapped counts data and summarise the transcripts-level data into
681 gene level data[57]. DESeq2 and SARTools packages[58], were used for differential gene expression
682 analysis, using a false discovery rate (FDR) <0.05, following normalisation with a negative binomial
683 generalised linear model. In addition, transcript abundance for protein coding genes was expressed
684 as $\log_2$-transformed transcripts per million (TPM) by normalising the read counts to gene length and
685 then read depth. Transcriptomes from nasal samples ranged from 16 to 66 million reads per sample
686 and in principle component analysis, revealed a batch effect that was corrected by the Combat
687 function in the Surrogate Variable Analysis (SVA) R/Bioconductor package (Supplementary
688 Figure)[59].

689

690 Identification of interacting networks and pathway enrichment analysis was performed using XGR R
691 package[60]. Interacting genes (supported by at least one experimental source of evidence) were
692 identified from the Pathway Commons database for directed interactions (Supplementary File).
693 These were then subjected to Reactome pathway enrichment analysis with FDR<0.05
694 (Supplementary File). K-means clustering of Jaccard indices to quantify similarity between the
695 composition of genes mapping to each pathway was used to identify 20 groups of pathways, from
696 which the pathway consisting of the largest total number of genes was selected to provide a
697 representative annotation for each group. The expression of gene modules in the nasal
698 transcriptomes was represented by the mean $\text{Log}_2$ TPM value of the genes in each module.

699

700 **Code Availability**

701 Codes used to process the RNAseq data can be found at https://github.com/cristina86cristina.

702

703 **Statistics**

704 All experiments were conducted with replicates in three or more independent experiments unless
705 stated otherwise. Error bars represent SEM unless stated otherwise. GraphPad Prism Version 10
706 was used to perform two-tailed parametric (t-tests or ANOVA) or non-parametric (Mann-Whitney or
707 Kruskal-Wallis tests) analysis, which was based on the Shapiro-Wilk normality test. P values less
708 than 0.05 were considered significant and are derived from non-parametric statistical tests unless
709 stated otherwise.

710

711

712

713

714 **FIGURE LEGENDS**

715

716 **Table 1. *Streptococcus pneumoniae* association with the nasal epithelium in the EHPC model**
717 **detected by culture, confocal microscopy and LytA PCR**

718 Nasal washes and nasal curette biopsies were collected from carriage positive and carriage negative
719 volunteers over time. Standard methods for measuring bacterial density by culture (CFU) and LytA
720 PCR were compared against counts visualised by confocal microscopy for pneumococcal
721 association with nasal cells over time. The data was derived from 13 volunteers. + (1-10
722 pneumococci); ++ (11-50 pneumococci); +++ (51-100 pneumococci); ++++ (>100 pneumococci); n/a
723 = reading not taken.

724

725 **Figure 1. *Streptococcus pneumoniae* colonisation of the human nasal epithelium from the**
726 **EHPC model is associated with adhesion, microcolony formation and micro-invasion in**
727 **response to *S. pneumoniae* 6B colonisation**

728 (a) Representative fields from the EHPC model nasal curette biopsies show intact epithelium can be
729 obtained from the samples (as visualised by XY planes) and they retain their size and shape (as
730 visualised by XZ planes). Cells were stained with Wheat Germ Agglutinin (WGA) or Junctional

731 Adhesion Molecule -A (JAM-A, red) and nuclei. (b) The pattern of pneumococcal density detected
732 by culture and microscopy. (c) The proportion of bacteria located on the cell surface, intracellularly,
733 or paracellularly visualised by confocal microscopy, quantified from 8 volunteers collected over time
734 from microscopy counts. (d) Cells were stained for surface carbohydrates using WGA (red), and the
735 bacteria were marked with specific serotype antiserum (green). XY images of 1µm slices through a
736 layer of cells, with bacteria associated. (e) Examples of cells showing; (ei) Microcolony formation on
737 the surface of the epithelium, (eii) bacterial internalization, (eiii) migration through epithelial uptake
738 internally or between cells. (f) Co-association between *S. pneumoniae* (green) and JAM-A (red).
739 Nuclei (blue). Bacterial uptake appeared co-associated with JAM-A (yellow).

740

741 **Figure 2. Epithelial surface marker expression is not altered in response *to S.***
742 ***pneumoniae* 6B colonisation *in vivo***

743 Epithelial cells from nasal curette biopsies were analysed by flow cytometry for (a) CD54 and (b)
744 CD107a. Results were expressed as median fluorescence intensity (left) and high cell surface
745 expression (≥95% of the baseline expression) representing at least two volunteers per time point
746 who were carriage negative (black) and carriage positive (grey).

747

748 **Figure 3. *Streptococcus pneumoniae* infection of nasopharyngeal epithelium *in vitro* is**
749 **associated with adhesion, microcolony formation, micro-invasion, transmigration and is**
750 **partially influenced by pneumolysin.**

751 (a) Pneumococcal association and (b) internalisation: Detroit 562 cell monolayers were stimulated
752 with pneumococci for 1 or 3 hours and the quantity of associated bacteria was determined by culture
753 (CFU); n>3. (****P = <0.0001: (a) 1hr (dashed lines, ANOVA); 3hr (solid lines, Kruskall-Wallis); (b)
754 Kruskall-Wallis). (c) Pneumococcal transmigration: Cells on transwell inserts were stimulated with
755 pneumococci for 3 hours and bacterial density in the basal chamber was determined (**P = 0.0092,
756 Kruskall-Wallis). N = 5. (di) Representative pneumococcal-density (green) images of cells (blue

757 nuclei). Scale bar = 20μm. n > 3. (e - h) Representative images of pneumococcal localization (green)
758 from cells (red, JAM-A), illustrating: (e) differences in adherence by 6B and TIGR4; (f) internalised
759 bacteria co-localised with JAM-A with associated intracellular vesicle-like bodies (yellow); (g) lateral
760 localisation of pneumococci (XY images) with possible paracellular movement co-associated with
761 JAM-A (XZ images); (h) basal localisation of bacteria at the level of nuclei and insert pores. N = >20.

762

763 **Figure 4. Transmigration of *S. pneumoniae* is endocytosis-dependent but does not disrupt**
764 **barrier integrity or function**

765 (a and b) Detroit 562 cells were treated with dynasore and nystatin for 30 minutes prior to and during
766 incubation with 23F, for 1 hour. (a) Intracellular bacteria were quantified using a gentamicin
767 protection assay and CFUs counted (****P = <0.0001, Mann-Whitney). (b) Transmigrated bacteria
768 after one hour were counted by CFUs (*P = 0.013 Mann-Whitney). N = 4. (c and d) Cells were co-
769 infected with pneumococci for three hours on transwell inserts and barrier function was measured.
770 (c) TEER was compared before and after exposure to pneumococci. N = 9. Calcium withdrawal was
771 used as a positive control (***P = 0.0013, unpaired T-test, n = 3). (d) Permeability was assessed by
772 leak to 4kDa FITC-dextran, collected from basal chamber. N = >4. ****P = <0.0001 comparing non-
773 infected against pneumococci (Kruskall-Wallis). Blank inserts were used as a positive control (Mann-
774 Whitney).

775

776 **Figure 5. Epithelial CD107a and CD54 surface expression and secretion of IL-6, IL-8 and CD54**
777 **are upregulated after *S. pneumoniae* exposure *in vitro***

778 (a and b) Detroit 562 cells were stimulated with *S. pneumoniae* for 6 hours and the median
779 fluorescence intensity and high-expressing cells for (a) CD54 and (b) CD107a were analysed by flow
780 cytometry. n = >3 independent experiments (**** P < 0.0001 CD107a MFI, compared to non-infected
781 cells, ANOVA. *** P = 0.0009 for MFI CD107a, TIGR4 v dPly, unpaired T-test. *** P < 0.001 CD107a
782 high expression, compared to non-infected cells, ANOVA *P = 0.028 for high expression CD107a,
783 TIGR4 vs. dPly, Mann-Whitney). (* P = 0.048 NI v TIGR4; * P = 0.0367 NI v dPly for CD54, ANOVA).

784 (c) IL-6, IL-8 and CD54 in the supernatants from Detroit 562 cells stimulated with *S. pneumoniae* for
785 6 hours, were measured by ELISA. N = 6 independent experiments with replicates. (**** P <0.0001
786 IL-6; *** P = 0.0013 CD54; **** P < 0.0001 IL-8 (Kruskall-Wallis test)).

787

788 **Figure 6. The epithelial transcriptomic response to *Streptococcus pneumoniae in vitro* is**
789 **influenced by epithelial adhesion and micro-invasion**

790 (a) The total number of Detroit 562 epithelial genes upregulated following exposure to 6B, 23F,
791 TIGR4 and TIGR4-dPly pneumococci, compared to non-infected samples. N = 3 independent
792 experiments with replicates. Genes with an FDR <0.05 were considered for further analysis. The
793 matrix shows intersections for the four strains, sorted by size. Dark circles in the matrix indicates
794 sets that are part of the intersection (d) Bubble heat map showing the results of transcriptional factor
795 analysis in Opossum for each strain. Transcriptional factors are ordered by family and then sorted
796 by number of genes in the database. The colour represents the log2 z-scores (a continuum from
797 blue to red as before) and the size shows the number of genes annotated to the particular pathway.
798 (c) Bubble heat map showing the results of Reactome Pathway Analysis for upregulated genes in
799 each strain compared to non-infected cells. Pathways were clustered in 20 groups using K-means
800 on Jaccard index and the biggest pathway for each group was selected for representative annotation
801 of each cluster. Individual pathways within clusters are shown in Supplementary Figure 8. The colour
802 represents the log2 z-scores (a continuum from blue (lowest values) and red (highest values) and
803 the size shows the number of genes annotated to each pathway. (d) Selected bubble heat map
804 clusters representing the individual pathways within each cluster from (c).

805

806 **Figure 7. Epithelial-derived transcriptomic responses to *S. pneumoniae* in the EHPC model**
807 **correlate with bacterial clearance**

808 (a) Network representation generated from the *in vitro* analyses for each strain. From the genes
809 present in the networks, an integrated gene list (200 genes) and a core genes list (16 genes) were
810 generated and tested as modules in the *in vivo* data. (b and c) Upregulated genes in comparison to

811 the transcriptomes of carriage negative and carriage positive volunteers were compared between
812 time points. Plots represent log2 TPM arithmetic mean for genes in the core (b) and integrated (c)
813 modules. P = <0.05, (one tail Mann-Whitney test). Number of samples for carriage negative and
814 positive, respectively: pre (17:14), day 2 (15:14), day 9 (7:7).

815

816 **Figure 8. Model of the control of pneumococcal colonisation by the human mucosal**
817 **epithelium.**

818 Following pneumococcal adhesion and microcolony formation on the epithelial surface, the
819 host response is dependent on the subsequent pattern of interaction. Micro-invasion
820 (endocytosis and paracellular transmigration) amplifies epithelial sensing and inflammation/
821 innate immunity, which we postulate leads to immune cell engagement. This process of
822 epithelial sensing inflammation/ innate immunity may enhance both transmission and
823 clearance. Co-association with junctional proteins may facilitate migration across the barrier.

824

# Table 1

| | | Sample day | | | | | Pneumococcal association | | |
|---|---|---|---|---|---|---|---|---|---|
| **ID** | **Pneumococcal density** | **Pre** | **D2** | **D6** | **D9** | **D27** | **Surface** | **Intracellular** | **Lateral** |
| **1** | **Culture (CFU/ml)** | 0 | 373 | 520 | 10 | 2 | | | |
| | **Microscopy (counts)** | 0 | + | + | 0 | + | + | 0 | 0 |
| | **LytA PCR** | NEG | POS | POS | n/a | POS | | | |
| **2** | **Culture (CFU/ml)** | 0 | 0 | 0 | 0 | 0 | | | |
| | **Microscopy (counts)** | + | + | 0 | 0 | 0 | ++ | + | 0 |
| | **LytA PCR** | NEG | NEG | NEG | n/a | NEG | | | |
| **3** | **Culture (CFU/ml)** | 0 | 0 | 0 | 0 | 0 | | | |
| | **Microscopy (counts)** | 0 | + | 0 | 0 | 0 | + | 0 | 0 |
| | **LytA PCR** | NEG | POS | NEG | n/a | NEG | | | |
| **4** | **Culture (CFU/ml)** | 0 | 3 | 9 | 0 | 0 | | | |
| | **Microscopy (counts)** | 0 | 0 | 0 | + | 0 | + | 0 | 0 |
| | **LytA PCR** | NEG | POS | POS | n/a | NEG | | | |
| **5** | **Culture (CFU/ml)** | 0 | $7x10^3$ | 223 | 22 | 0 | | | |
| | **Microscopy (counts)** | 0 | + | + | + | 0 | + | + | 0 |
| | **LytA PCR** | n/a | n/a | n/a | n/a | n/a | | | |
| **6** | **Culture (CFU/ml)** | 0 | $1.9x10^4$ | $5.7x10^3$ | $3.7x10^4$ | 11 | | | |
| | **Microscopy (counts)** | 0 | ++ | ++++ | ++ | 0 | +++ | ++ | + |
| | **LytA PCR** | NEG | POS | POS | n/a | POS | | | |
| **7** | **Culture (CFU/ml)** | 0 | 822 | $1.1x10^3$ | 160 | 0 | | | |
| | **Microscopy (counts)** | 0 | + | +++ | ++ | 0 | ++ | + | + |
| | **LytA PCR** | NEG | POS | POS | n/a | NEG | | | |
| **8** | **Culture (CFU/ml)** | 0 | 0 | 0 | 0 | 0 | | | |
| | **Microscopy (counts)** | 0 | 0 | 0 | 0 | 0 | 0 | 0 | 0 |
| | **LytA PCR** | n/a | n/a | n/a | n/a | n/a | | | |
| **9** | **Culture (CFU/ml)** | 0 | 221 | 695 | 4 | <1 | | | |
| | **Microscopy (counts)** | n/a | + | +++ | + | n/a | +++ | + | + |
| | **LytA PCR** | NEG | POS | POS | n/a | NEG | | | |
| **10** | **Culture (CFU/ml)** | 0 | $1x10^3$ | 0 | 0 | 0 | | | |
| | **Microscopy (counts)** | n/a | 0 | + | 0 | n/a | + | 0 | 0 |
| | **LytA PCR** | NEG | POS | POS | n/a | POS | | | |
| **11** | **Culture (CFU/ml)** | 0 | $1.8x10^6$ | $1.8x10^6$ | $1.9x10^4$ | <1 | | | |
| | **Microscopy (counts)** | n/a | ++++ | ++++ | + | n/a | +++ | + | + |
| | **LytA PCR** | NEG | POS | POS | n/a | NEG | | | |
| **12** | **Culture (CFU/ml)** | 0 | 0 | 0 | 0 | 0 | | | |
| | **Microscopy (counts)** | NR | ++ | 0 | 0 | n/a | ++ | + | + |
| | **LytA PCR** | NEG | NEG | NEG | n/a | NEG | | | |
| **13** | **Culture (CFU/ml)** | 0 | 23 | 2 | 0 | 0 | | | |
| | **Microscopy (counts)** | n/a | + | 0 | 0 | n/a | + | 0 | 0 |
| | **LytA PCR** | POS | POS | POS | n/a | POS | | | |

# Figure 1

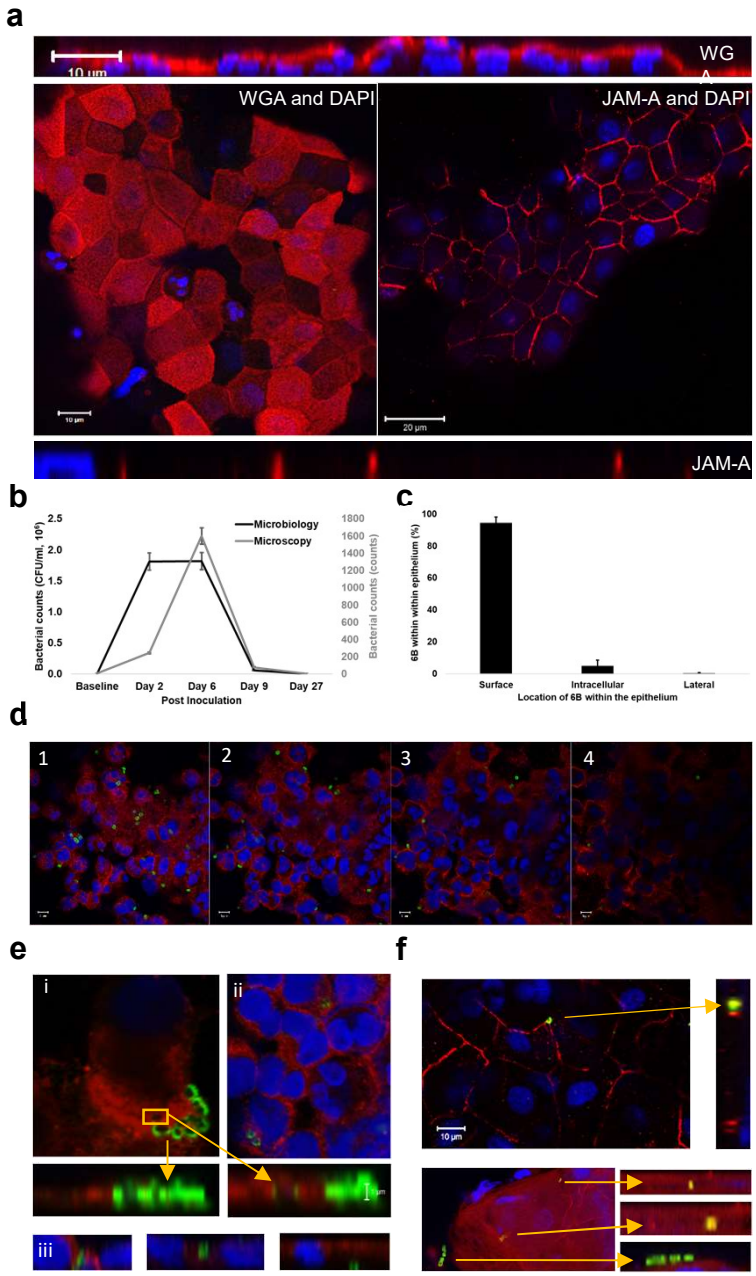
a
10 µm
WGA and DAPI
JAM-A and DAPI
20 µm
JAM-A
b
Microbiology
Microscopy
Bacterial counts (CFU/ml, 10⁶)
Bacterial counts (counts)
Baseline
Day 2
Day 6
Day 9
Day 27
Post Inoculation
c
6B within within epithelium (%)
Surface
Intracellular
Lateral
Location of 6B within the epithelium
d
1
2
3
4
e
i
ii
iii
f
10 µm

# Figure 2

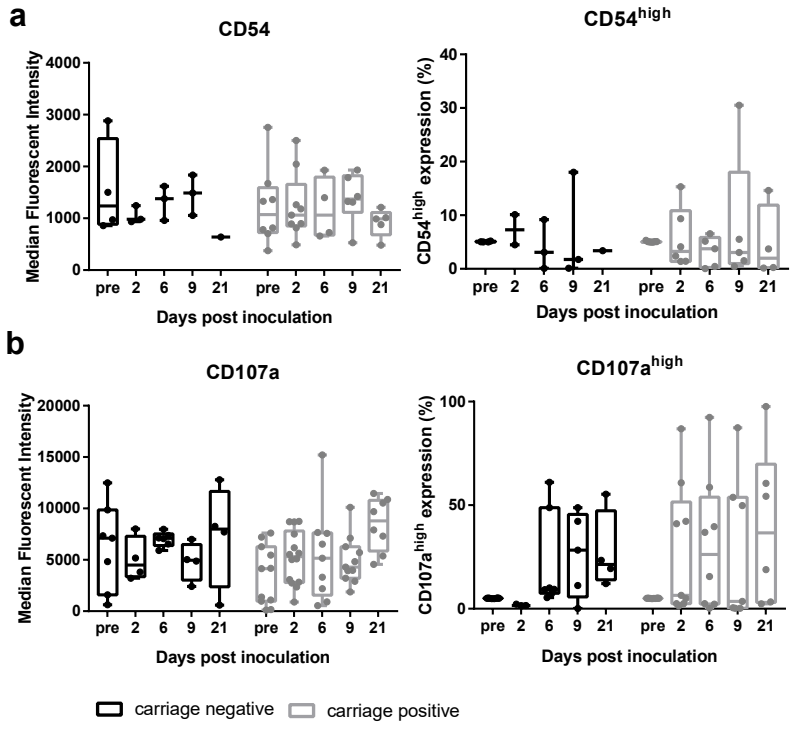
a
CD54
Median Fluorescent Intensity
4000
3000
2000
1000
0
pre 2 6 9 21 pre 2 6 9 21
Days post inoculation
CD54high
CD54high expression (%)
40
30
20
10
0
pre 2 6 9 21 pre 2 6 9 21
Days post inoculation
b
CD107a
Median Fluorescent Intensity
20000
15000
10000
5000
0
pre 2 6 9 21 pre 2 6 9 21
Days post inoculation
CD107ahigh
CD107ahigh expression (%)
100
50
0
pre 2 6 9 21 pre 2 6 9 21
Days post inoculation
carriage negative
carriage positive

# Figure 3

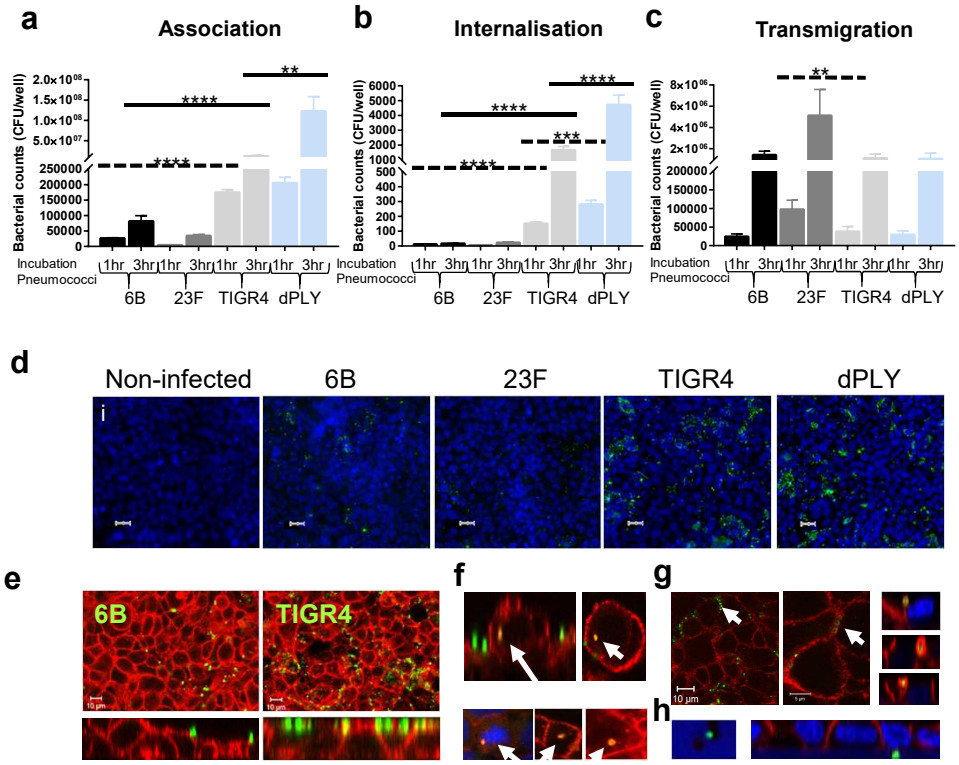
a
Association
b
Internalisation
c
Transmigration
Bacterial counts (CFU/well)
Incubation
Pneumococci
1hr 3hr 1hr 3hr 1hr 3hr 1hr 3hr
6B 23F TIGR4 dPLY
****
**
***
d
Non-infected
6B
23F
TIGR4
dPLY
e
6B
TIGR4
f
g
h

# Figure 4

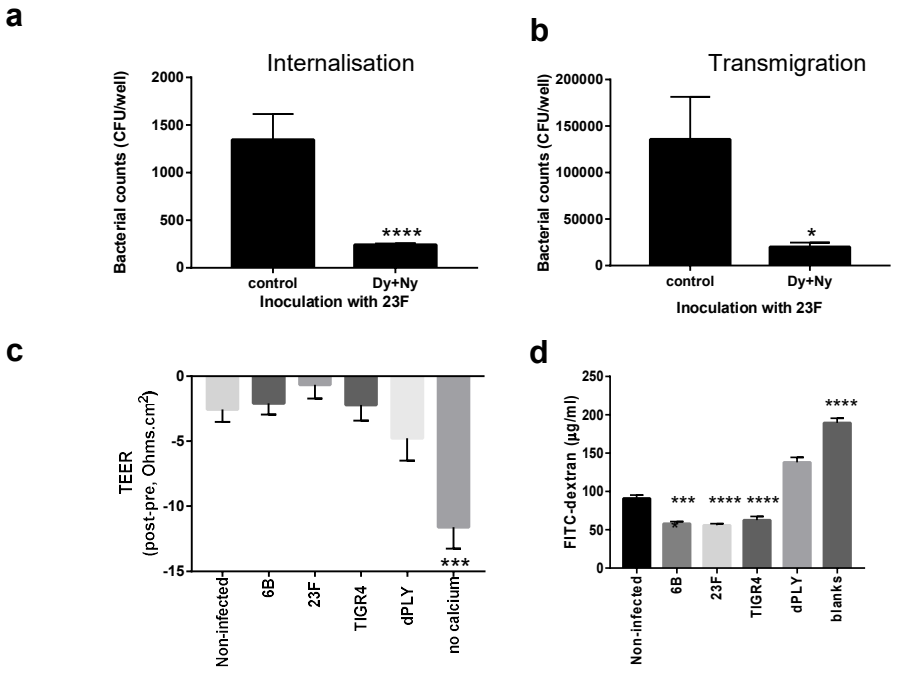
a
Internalisation
Bacterial counts (CFU/well)
2000
1500
1000
500
0
****
control
Dy+Ny
Inoculation with 23F
b
Transmigration
Bacterial counts (CFU/well)
200000
150000
100000
50000
0
*
control
Dy+Ny
Inoculation with 23F
c
TEER
(post-pre, Ohms.cm2)
0
-5
-10
-15
***
Non-infected
6B
23F
TIGR4
dPLY
no calcium
d
FITC-dextran (µg/ml)
250
200
150
100
50
0
***
****
****
****
Non-infected
6B
23F
TIGR4
dPLY
blanks

# Figure 5

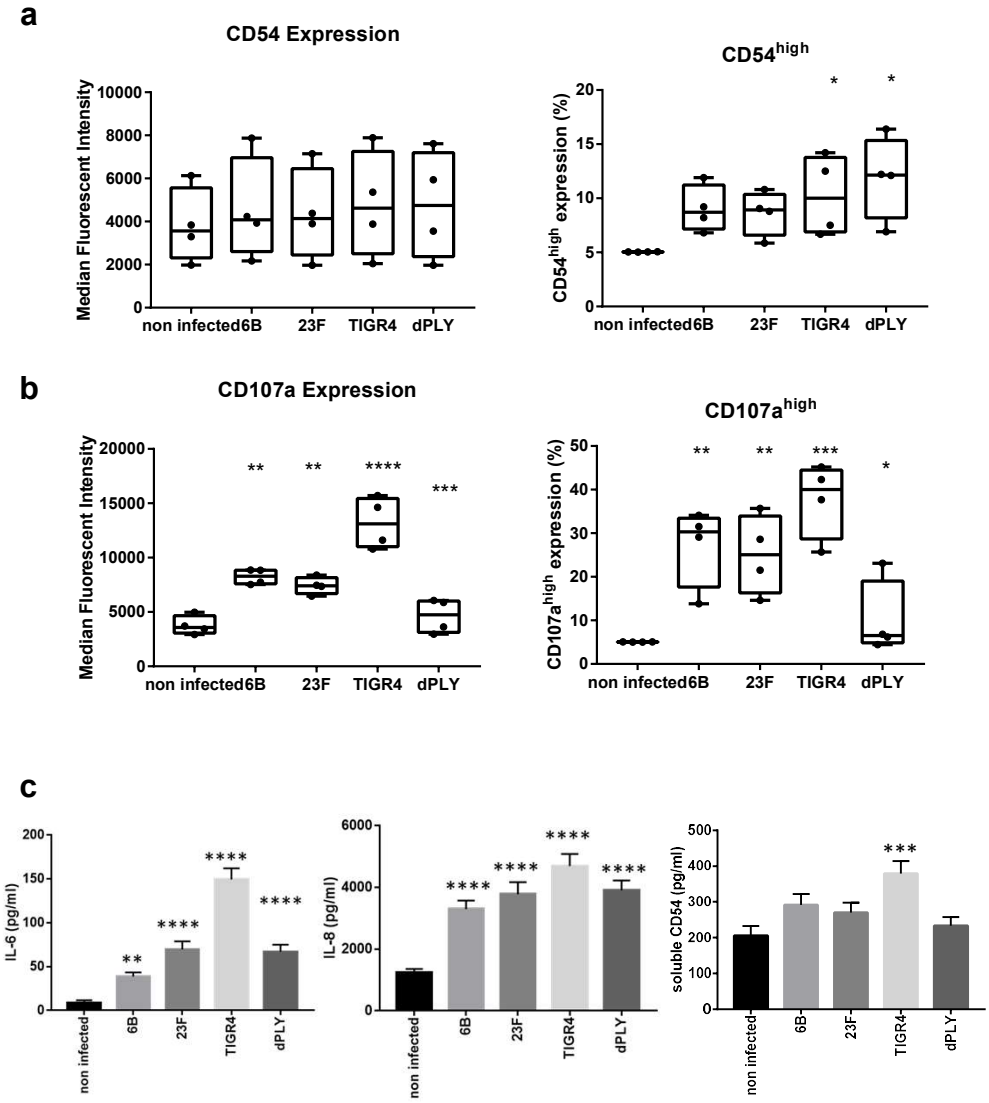
a
CD54 Expression
Median Fluorescent Intensity
10000
8000
6000
4000
2000
0
non infected
6B
23F
TIGR4
dPLY
CD54high
CD54high expression (%)
20
15
10
5
0
*
*
b
CD107a Expression
Median Fluorescent Intensity
20000
15000
10000
5000
0
**
**
****
***
CD107ahigh
CD107ahigh expression (%)
50
40
30
20
10
0
**
**
***
*
c
IL-6 (pg/ml)
200
150
100
50
0
**
****
****
****
IL-8 (pg/ml)
6000
4000
2000
0
****
****
****
****
soluble CD54 (pg/ml)
500
400
300
200
100
0
***
non infected
6B
23F
TIGR4
dPLY

# Figure 6

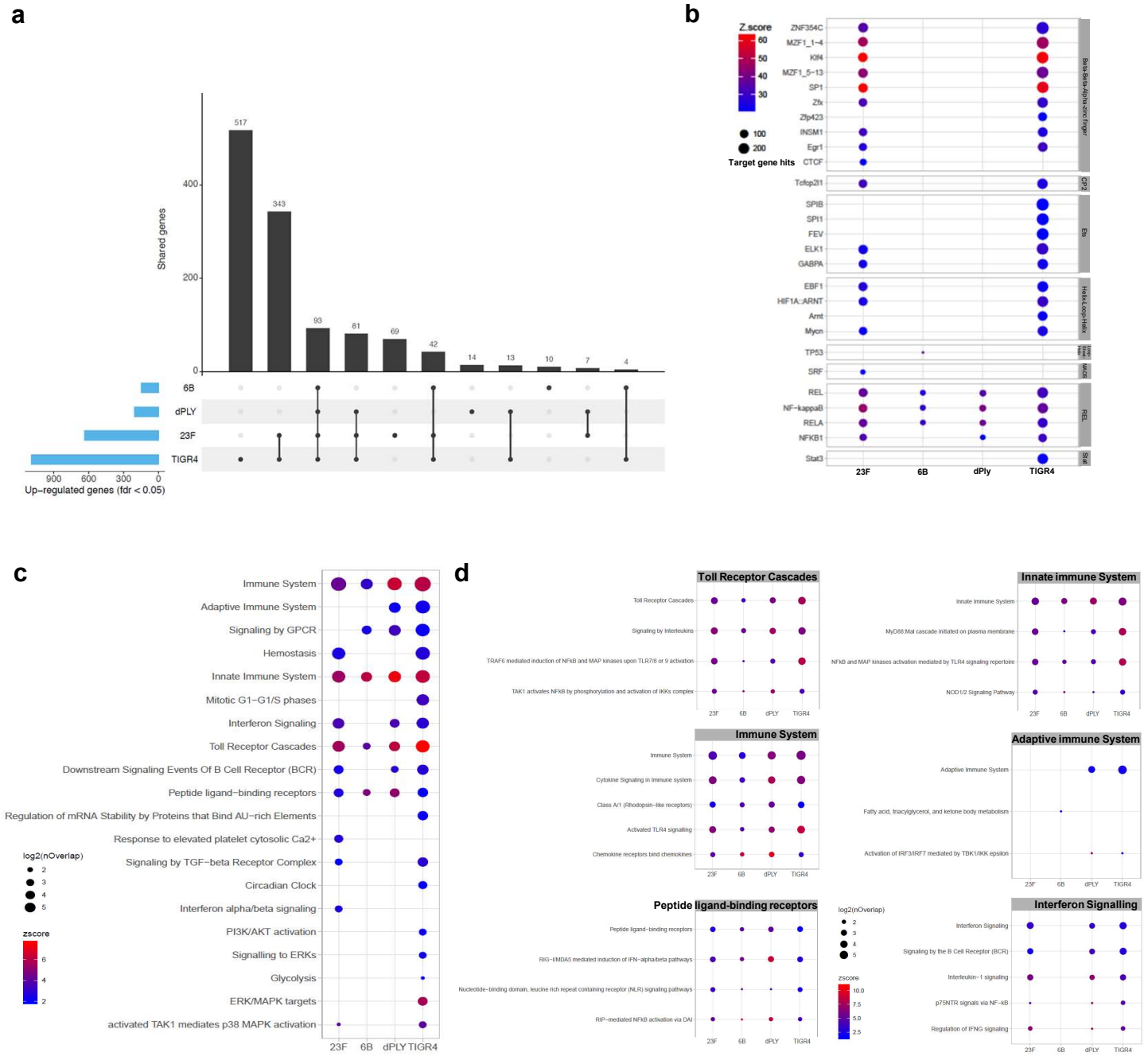
a
Shared genes
517
343
93
81
69
42
14
13
10
7
4
6B
dPLY
23F
TIGR4
Up-regulated genes (fdr < 0.05)
b
Z.score
Target gene hits
ZNF354C
MZF1_1-4
Klf4
MZF1_5-13
SP1
Zfx
Zfp423
INSM1
Egr1
CTCF
Tcfcp2l1
SPIB
SPI1
FEV
ELK1
GABPA
EBF1
HIF1A::ARNT
Arnt
Mycn
TP53
SRF
REL
NF-kappaB
RELA
NFKB1
Stat3
23F
6B
dPly
TIGR4
c
Immune System
Adaptive Immune System
Signaling by GPCR
Hemostasis
Innate Immune System
Mitotic G1-G1/S phases
Interferon Signaling
Toll Receptor Cascades
Downstream Signaling Events Of B Cell Receptor (BCR)
Peptide ligand-binding receptors
Regulation of mRNA Stability by Proteins that Bind AU-rich Elements
Response to elevated platelet cytosolic Ca2+
Signaling by TGF-beta Receptor Complex
Circadian Clock
Interferon alpha/beta signaling
PI3K/AKT activation
Signalling to ERKs
Glycolysis
ERK/MAPK targets
activated TAK1 mediates p38 MAPK activation
log2(nOverlap)
zscore
23F
6B
dPLY
TIGR4
d
Toll Receptor Cascades
Innate immune System
Immune System
Adaptive immune System
Peptide ligand-binding receptors
Interferon Signalling

# Figure 7

**a**

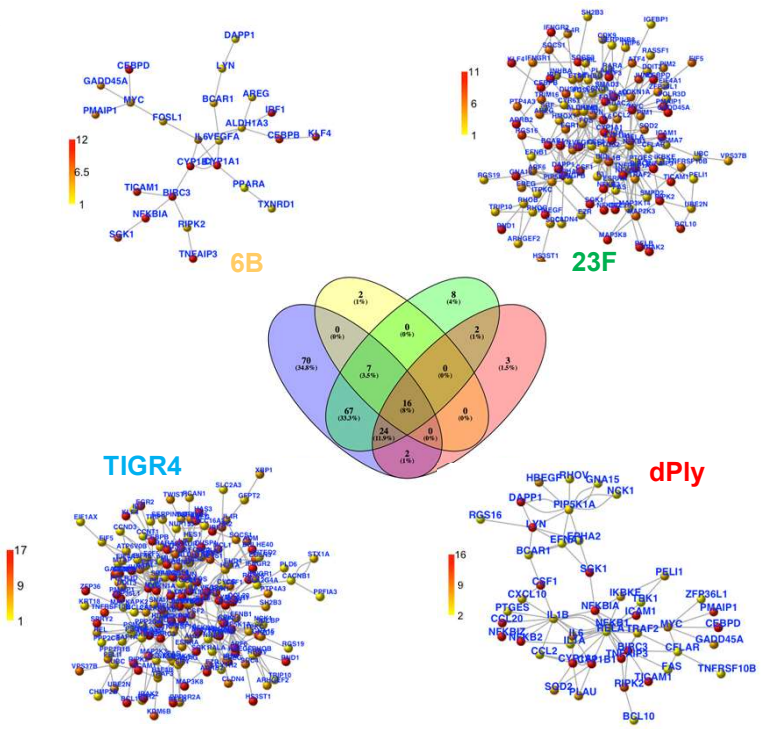
6B
23F
TIGR4
dPly

**b**

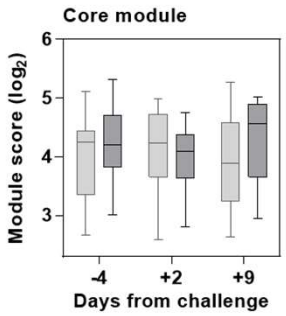
Core module
Module score (log2)
Days from challenge
-4
+2
+9

**c**

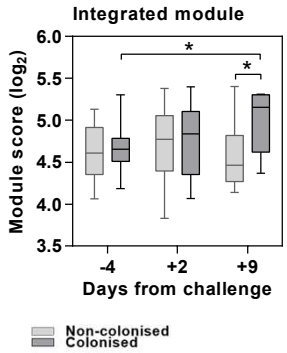
Integrated module
Module score (log2)
Days from challenge
-4
+2
+9
Non-colonised
Colonised

**Figure 8**

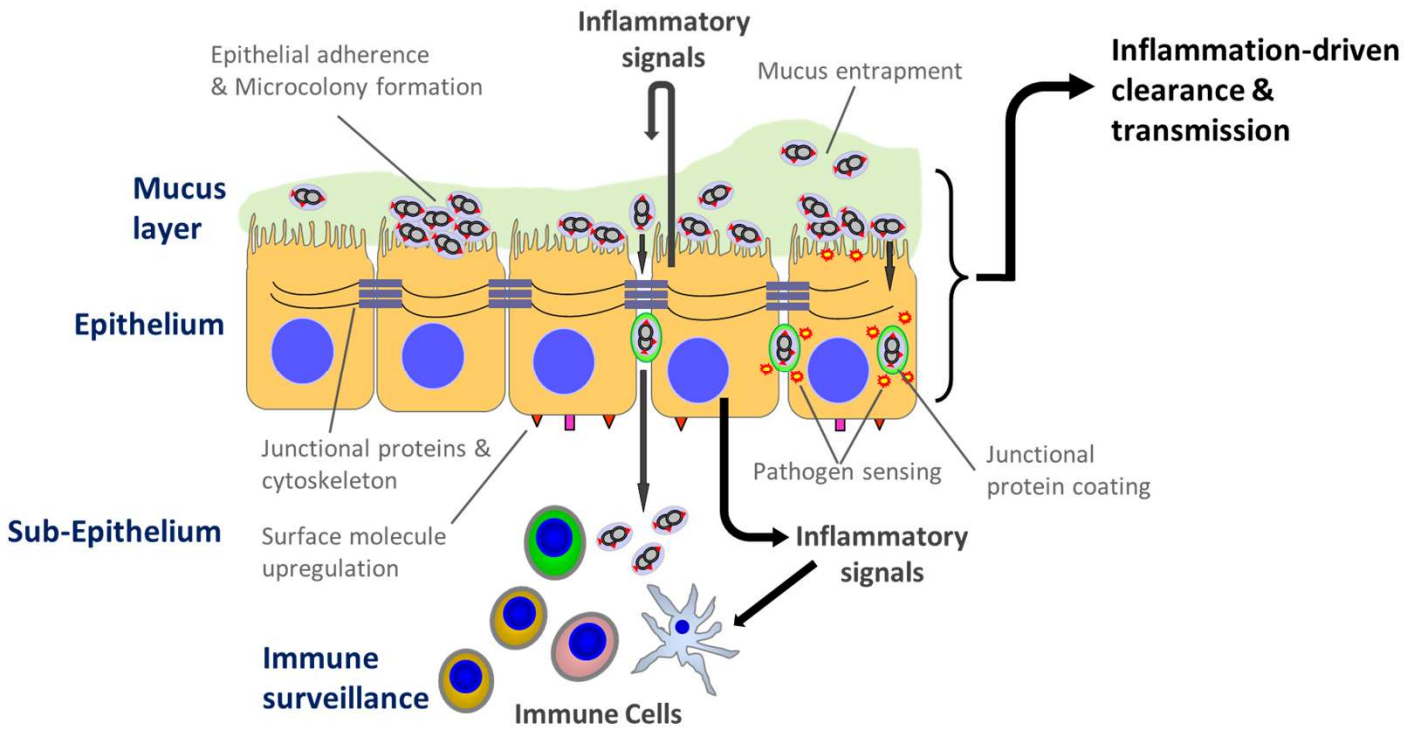
Inflammatory signals
Epithelial adherence & Microcolony formation
Mucus entrapment
Inflammation-driven clearance & transmission
Mucus layer
Epithelium
Junctional proteins & cytoskeleton
Pathogen sensing
Junctional protein coating
Sub-Epithelium
Surface molecule upregulation
Inflammatory signals
Immune surveillance
Immune Cells